Eur. Phys. J. B **36**, 281–287 (2003)
DOI: 10.1140/epjb/e2003-00345-6

THE EUROPEAN PHYSICAL JOURNAL B

Charge-carrier transport properties of ultrathin Pb films

I. Vilfan[1,a] and H. Pfnür[2]

[1] J. Stefan Institute, Jamova 39, SI-1001 Ljubljana, Slovenia
[2] Institut für Festkörperphysik, Universität Hannover, Appelstrasse 2, 30167 Hannover, Germany

Received 15 July 2003 / Received in final form 19 September 2003
Published online 8 December 2003 –

Abstract. The charge-carrier transport properties of ultrathin metallic films are analysed with ab initio methods using the density functional theory (DFT) on free-standing single crystalline slabs in the thickness range between 1 and 8 monolayers and compared with experiments for Pb films on Si(111). A strong interplay between bandstructure, quantised in the direction normal to the ultrathin film, charge-carrier scattering mechanisms and magnetoconduction was found. Based on the bandstructure obtained from the DFT, we used standard Boltzmann transport theory in two dimensions to obtain results for the electronic transport properties of 2 to 8 monolayers thick Pb(111) slabs with and without magnetic field. Comparison of calculations and experiment for the thickness dependence of the dc conductivity shows that the dominant scattering mechanism of electrons is diffuse elastic interface scattering for which the assumption of identical scattering times for all subbands and directions, used in this paper, is a good approximation. Within this model we can explain the thickness dependences of the electric conductivity and of the Hall coefficient as well as the anomalous behaviour of the first Pb layer.

PACS. 73.50.Jt Electronic transport phenomena in thin films: Galvanomagnetic and other magnetotransport effects – 73.61.At Electrical properties of specific thin films: Metals and metallic alloys – 73.20.At Electron states at surfaces and interfaces – 71.15.Mb Density functional theory

1 Introduction

Spatial confinement of the electron motion in the direction normal to the film causes quantisation of the perpendicular momentum and consequently a discrete set of electron energy subbands. This leads to a variety of quantum-size effects (QSE), like oscillation of the charge-carrier density, Fermi energy, electrical conductivity and of the Hall coefficient as a function of film thickness, to mention only a few of them. Although appreciable progress has been made in understanding the QSE, many aspects are still unclear. Here we will discuss the electronic band structure and its consequences on the electronic charge transport with and without magnetic field in ultrathin films.

The *classical* size effect on the conductivity of thin films is explained with the Fuchs and Sondheimer theories [1–3] which relate the electrical conductivity in the film and surface or interface scattering. Their approach is based on the Boltzmann transport equation for *bulk* electrons that are partially reflected and partially scattered on the film surfaces. Assuming *diffuse* and *elastic* surface scattering they find a linear thickness dependence of the conductivity, often in agreement with experiments even for film thicknesses d much smaller than the electron elastic mean free path ℓ, although the picture of 3-dimensional electron motion with specular reflections at the surface or interface makes sense only when $d \gg \ell$. A linear d-dependence of the conductivity has also been obtained by Camblong and Levy [4], who used the Kubo formalism and assumed a free-electron model with diffuse scattering on the boundaries.

A *quantum* size effect is the oscillation of the conductivity with thickness d, observed in the layer-by-layer growth mode of thin films. These oscillations have the period of the perpendicular lattice spacing and are caused by the roughness of films with partial monolayers that are not closed. For film thicknesses $d \ll \ell$ the discrete nature of the electron energy levels becomes essential and other quantum-size induced effects emerge on top of the layer-by-layer induced oscillations. The transport of free electrons in confined geometries has been discussed by Sandomirskii [5] and later by Trivedi and Ashcroft [6]. They predicted a saw-tooth like oscillations of the in-plane conductivity with thickness. The period of the oscillation is equal to half the Fermi wavelength λ_F [6]. In reality, however, the film thickness increases in monolayer steps and not continuously as assumed in the above models. Therefore, one expects a range of thicknesses with large

[a] e-mail: igor.vilfan@ijs.si

QSE amplitudes when d is close to a multiple of $\lambda_F/2$, separated by regions with small QSE.

Apart from the theoretical attempts mentioned above, there have been several others which describe charge transport in thin films [7–13]. Common to most of them is the assumption of free electrons. However, models based on free electrons break down if they are used to explain the galvanomagnetic phenomena (like the Hall effect), which depend on details of the band structure and on the electron/hole ratio, as will be shown below. More quantitative models are needed that take into account the detailed band structure of the film under size quantisation.

In this paper we address the general issue of charge-carrier scattering, transport and Hall effect in ultrathin metallic films. The Hall *coefficient* has the advantage that it is more sensitive to the QSE-mediated changes in the bandstructure and less sensitive to the details of the scattering mechanisms than the electrical or Hall *conductivities*. The model calculations will be performed on free-standing Pb(111) slabs and compared with experiments for Pb on Si(111). As substrates, semiconductors are used because they have no electron states at the Fermi energy to which the metal conduction electrons, responsible for the charge transport, could couple. Semiconductors are also good insulators in the relevant temperature range (up to 150 K) so that they can be considered as an insulating substrate. Depending on substrate and annealing conditions, both crystalline and semi-amorphous films can be grown. This is important because it allows a comparison of magnetoconductive properties of crystalline and non-crystalline films. For the Hall coefficient the degree of crystallinity is of minor importance.

The bandstructure of free-standing ultrathin Pb(111) films has been calculated by Saalfrank [14] and more recently by Matrezanini et al. [15]. They discussed the role, QSE has on the oscillations of the Fermi energy ϵ_F and of the density of electron states n_F at ϵ_F but did not consider the charge-carrier transport phenomena. Charge transport properties at low temperatures are dominated by scattering at bulk and surface imperfections. For most ultrathin metallic films with $d < \ell$, scattering at the surface roughness is much stronger than scattering at bulk imperfections, the electrical conductivity is limited by roughness of the boundaries to the vacuum and to the substrate. The variation of the conductivity with thickness d of ultrathin rough metallic films has been investigated by Fishman and Calecki [9,10]. In case of free electrons and uncorrelated surface height fluctuations, they obtain a $d^{2.1}$ thickness dependence of the "residual" conductivity $\sigma = [\rho(d) - \rho(\infty)]^{-1}$, where $\rho(d)$ is the in-plane film resistivity, and a Hall coefficient R_H proportional to d. None of these dependences agrees with the experiments on ultrathin Pb films on Si(111), where an approximately linear thickness dependence of σ and a strongly oscillating thickness dependence of R_H has been reported [16–18].

2 The model

We treat metallic films as free-standing, ideally ordered slabs. The density functional theory (DFT) is applied to calculate the electronic band structure, density of states and Fermi lines. Using the Boltzmann transport equation in the relaxation time approximation and in two dimensions we then calculate the transport properties of ultrathin slabs. We will see that most of the charge-carrier transport properties as a function of layer thickness d are already reproduced in such approach.

The basis of our charge-transport calculations are the electron band structures. In a slab, the translational symmetry in the direction normal to the slab is broken, $k_\perp$ is no longer a good quantum number, and each band splits into d discrete *subbands*. One can imagine these subband states as standing waves between the two surfaces. Of course, the subbands transform into a continuum of surface-projected bulk band states in the limit $d \to \infty$.

The question arises, when do we have to treat the electron states as confined in a slab and when as bulk states. The decisive quantity is the electron *coherence length* ℓ_c. If $\ell_c \ll d$, it is equivalent to the *bulk mean free path* and is determined by bulk scattering centres. When the coherence length exceeds the slab thickness, $\ell_c > d$, the electrons between the two slab boundaries behave as standing waves in the normal direction and as extended states in the other two directions. Therefore, in case of ultrathin slabs, one has to distinguish between the electron coherence length in the direction normal to the film, ℓ_c, and the electron mean free path in the plane of the film, ℓ_{mfp}, which is predominantly limited by the surface roughness.

The DFT calculations were performed on 1 to 8 monolayers thick, (111)-oriented Pb slabs, separated by ∼10 Å of vacuum, and with periodic boundary conditions. If the vacuum layer were too thin, we would observe dispersion of the electron bands in the z direction. Indeed, we observed no dispersion in the occupied bands. The electron band energies and the total energy were calculated ab initio with the full-potential linearised augmented plane-wave method in the local-density approximation [19] as implemented in the WIEN2k code [20]. A mixed basis set of augmented plane waves plus local orbitals (APW+lo) [21] for low orbital momenta ($l \leq 2$) and linearised augmented plane waves (LAPW) for all the higher orbital momenta were used. The spin-orbit interaction was included selfconsistently by applying the second-variational method and using the scalar-relativistic eigenfunctions as basis [22]. The Pb muffin-tin radius was set to 2.6 a.u. and a tetrahedral mesh of about 600 k-points in the irreducible part of the Brillouin zone, Figure 1, was used in the self-consistent electronic structure calculations. The kinetic-energy cutoff was set to $E^{\rm wf}_{\rm max} = 9.5$ Ry and the plane-wave expansion cutoff to $E^{\rm pw}_{\rm max} = 196$ Ry. Later, in the calculation of Fermi lines and conductivities, we used a mesh with about 4000 k points in the irreducible part of the Brillouin zone.

First, the energy of bulk Pb FCC crystal was minimised to find the equilibrium bulk lattice constant, $a_{\rm calc} = 4.88$ Å, which is 1.4% smaller than the experimental room-temperature value $a_{\rm exp} = 4.95$ Å and 3% smaller than the calculated value reported by Materzanini et al. who used the Cambridge Serial Total Energy Package [15]. For the slab calculations, we used the corresponding

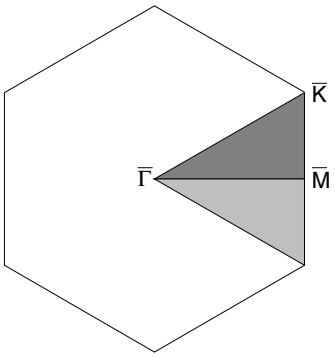

Fig. 1. Irreducible part (dark grey) of the two-dimensional hexagonal first Brillouin zone of a free-standing slab. For the slab on a substrate the in-plane mirror symmetry is broken and the irreducible Brillouin zone comprises both grey areas.

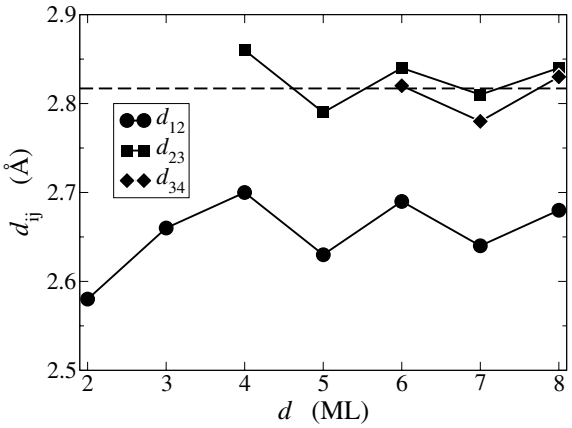

Fig. 2. Interlayer spacings d_{ij} (in Å) of relaxed symmetric Pb(111) slabs as a function of slab thickness. The lowest indices correspond to the surface layers. Dashed line indicates the relaxed bulk spacing.

in-plane hexagonal lattice constant, $a = a_{\mathrm{calc}}/\sqrt{2} = 3.45$ Å. Except for $d = 1$ ML, no visible change in the bandstructure is observed if either the experimental lattice constant was used in the simulations or if the lattice was unrelaxed.

The transport properties are calculated using the Boltzmann transport equation for two-dimensional systems in the relaxation-time approximation. The two-dimensional description is necessary when the charge-carrier mean free path exceeds the slab thickness. As we shall see later, this condition is fulfilled for all but the thinnest ($d = 1$) slabs. For polycrystalline or amorphous metallic films the transport properties are *isotropic* in the plane of the surface and the conductivity is [23]

$$\sigma_0 = \frac{e^2}{4\pi^2\hbar d} \sum_n \oint \mathrm{d}\ell_n \, \tau_n(\epsilon_F) |\boldsymbol{v}_n(\epsilon_F)| \qquad (1)$$

where e is the electron charge, $\boldsymbol{v}_n$ the group velocity of an electron in the subband n at the Fermi energy ϵ_F and $\tau_n(\epsilon_F)$ its relaxation time. The sum runs over all subbands crossing the Fermi energy and the integral is along each Fermi line. The spin degeneracy is included in the prefactors. The Hall conductivity is [23]

$$\sigma_H = \frac{e^3}{(2\pi\hbar)^2 d} \sum_n \tau_n^2(\epsilon_F) \oint \mathrm{d}\ell_n \frac{1}{|\boldsymbol{v}_n(\epsilon_F)|} \times \left(v_x^2 \frac{\partial v_y}{\partial k_y} + v_y^2 \frac{\partial v_x}{\partial k_x} \right). \qquad (2)$$

The mechanisms influencing the relaxation time are elastic scattering on bulk imperfections and elastic scattering on rough surfaces, $1/\tau = 1/\tau_b + 1/\tau_s$. Inelastic scattering on phonons can be neglected if the conductivities are investigated at low temperatures. In ultrathin films, the main scattering mechanism is elastic scattering on surface roughness for which $\tau_n(\epsilon_F)$ is given by

$$\frac{1}{\tau_n(\epsilon_F)} = \frac{2\pi}{\hbar} \sum_{n'k'} |\langle n'k'|\mathcal{H}_i|nk\rangle|^2 \delta(\epsilon_{n'}(k') - \epsilon_F) \qquad (3)$$

where $\langle n'k'|\mathcal{H}_i|nk\rangle$ is the scattering matrix element. For small, uncorrelated islands, the matrix element is independent of n and k, it is equal to $U^2\rho_s/Sd^2$ where U is the strength and ρ_s the surface density of the scattering centres [10]. S is the area of the film. If this situation is fulfilled, the scattering is *diffuse* [4] and the scattering rate simplifies to

$$\frac{1}{\tau} = \frac{U^2\rho_s}{2\pi\hbar^2 d^2} \sum_n \oint \frac{\mathrm{d}\ell_n}{|v_n(\epsilon_F)|}. \qquad (4)$$

In this case the charge-carrier momentum is lost completely, scattering causes transitions between all subbands that cross ϵ_F and also the relaxation time of the electrons at ϵ_F is *independent* of the subband index n and electron momentum k. In general, v_F is only weakly k-dependent so that $\tau \propto d^2/L$ results, where L is the length of all Fermi lines. As we shall see later, L and therefore also τ and σ_0 are approximately linear functions of d.

3 Results

We start our analysis by presenting the results of the lattice relaxation and bandstructure calculations of relaxed Pb(111) slabs. The thickness dependence of the interlayer spacings is shown in Figure 2. The topmost layer relaxes always inwards. In addition, we find a quantum-size induced oscillation of d_{ij} as a function of thickness; we observe simultaneous inward relaxation of all investigated layers for $d = 2$, 5 and 7 ML thick films. Whereas the relaxations of the topmost layers agree quite well with the values reported in reference [15], the relaxations of the inner layers differ. Our spacings d_{23} show similar QSE oscillations as in reference [15], but they are systematically smaller ($\sim$2% of d_{bulk}, d_{bulk} is the bulk interlayer spacing in the (111) direction). The amplitude of the QSE oscillations in d_{34} is $\sim$1.5% of d_{bulk} and is thus comparable to the amplitude of d_{34} in reference [15], but with opposite phases as a function of layer thickness.

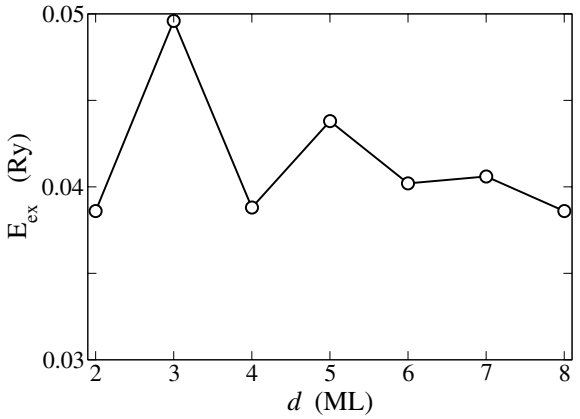

Fig. 3. Thickness dependence of the excess slab energies $E_{\rm ex}$ of relaxed symmetric Pb(111) slabs.

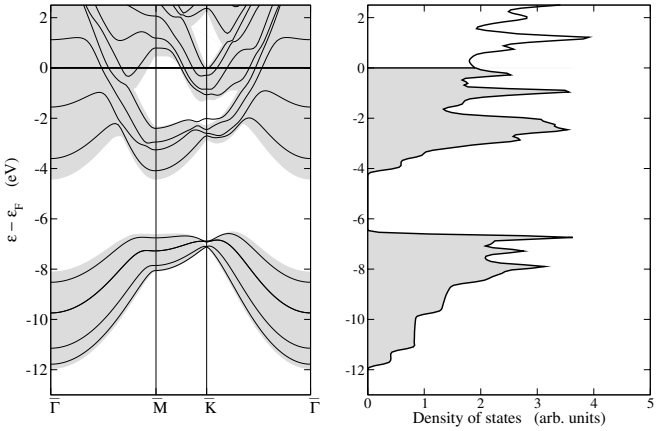

Fig. 4. Calculated bandstructure (left) and density of states (right) of a free-standing 4 ML thick Pb(111) film. The shaded areas in the bandstructure represent the surface-projected bulk electron energy bands, whereas the shaded areas in the density-of-states are the occupied states of the 4 ML thick Pb film.

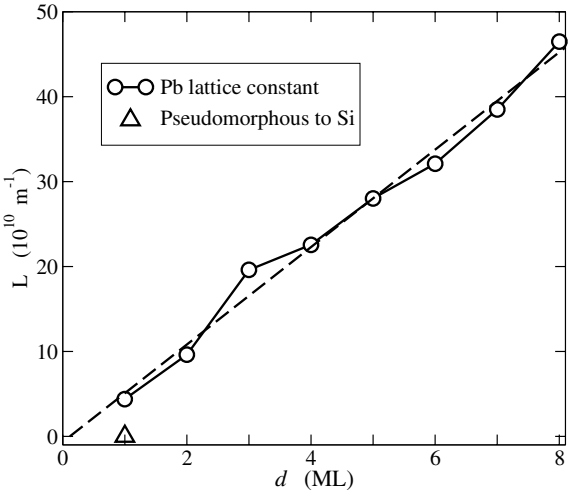

Fig. 5. Thickness dependence of the total length L of calculated Fermi lines in the two-dimensional Brillouin zone. Dashed line is a linear fit through the the calculated points. Also shown is the calculated Fermi-line length of a $d = 1$ ML thick film, pseudomorphous with the Si(111) substrate.

Figure 3 shows the excess slab energies $E_{\rm ex} = E_{\rm slab} - dE_{\rm bulk}$, where $E_{\rm slab}$ is the total energy of a slab and $E_{\rm bulk} = -41834.809$ Ry the energy/atom in the bulk. Clearly seen are the QSE-induced oscillations in $E_{\rm ex}$ with minima for 2, 4 and presumably also 8 ML thick slabs, in partial agreement with the DFT calculations of reference [15].

The electron energy bands along the main symmetry directions of the two-dimensional hexagonal Brillouin zone for $d = 4$ are shown in Figure 4. Each band is split into d subbands which do not cross because of spin-orbit interaction. The number of subbands crossing ϵ_F is roughly proportional to d. This property will have direct consequences on τ and on the conductivities. The points of subband crossings with ϵ_F form two-dimensional closed loops, i.e., Fermi lines. Depending on the occupancy of the states enclosed by a Fermi line we have hole- or electron-like carriers. Their ratio will play a crucial role in determining the sign of the Hall coefficient $R_H = \sigma_H/\sigma_0^2$. Also shown in Figure 4 is the electron density of states. Close to the bottom of the subbands the density of states has steps, specific for parabolic bands in two dimensions. Proportional to d is also the total length of Fermi lines, L, in the two-dimensional Brillouin zone, see Figure 5. This, together with diffuse scattering, is the main reason why σ_0 is approximately proportional to d.

We next calculated the relaxation time, equation (4), assuming a potential depth 3 eV, a terrace height one ML ($\sim$3 Å), a terrace area 100 Å^2 ($U = 900$ eVÅ^3) and a terrace density $\rho_s = 10^{-4}$ Å^{-2}, see Figure 6. These numbers were chosen in order to simulate closely the experimental situation described in reference [24] and to obtain a close fit to the experimental values for σ_0 and R_H [24]. We note that elastic scattering at the surfaces causes transitions between *all* subbands that cross the Fermi energy. The summation over all final states in the scattering rate (4) causes $\tau \propto d$. As we see from Figure 6, $\tau \propto d-1$ describes the thickness dependence better. The reason is found in the details of the bandstructure (see below). The deviations from linearity at $d = 3$, 6 and 8 ML appear when the Fermi energy coincides with a local peak in the electron density of states, thus opening more channels for elastic scattering. Also shown in Figure 6 is the "experimental" value $\tau^{\rm exp}$,

$$\tau^{\rm exp} = \frac{4\pi^2\hbar d\,\sigma_0^{\rm exp}}{e^2 \oint dl|v_n(\epsilon_F)|}, \qquad (5)$$

obtained from equation (1) by combining $\sigma_0^{\rm exp}$ from reference [18] with the calculated value for $\oint dl|v_n(\epsilon_F)|$. We also calculated σ_0, Figure 7, and σ_H, Figure 8. σ_0 has a very similar thickness dependence as τ, indicating, that τ is the main source of the thickness dependence of σ_0.

The Hall conductivity, σ_H, on the other hand, is a complicated function of d, mainly because of compensating effect of electron and hole subbands contributions.

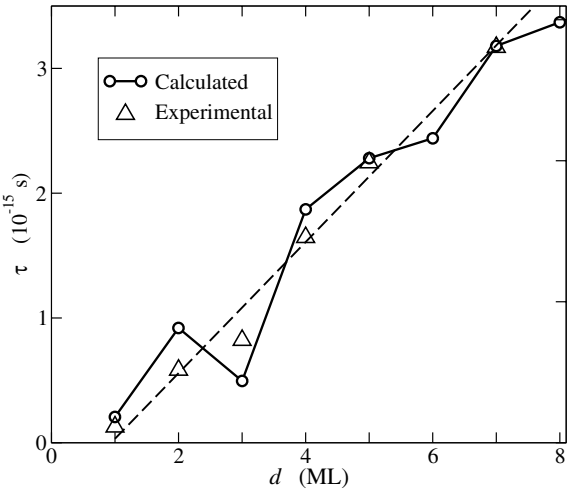

Fig. 6. Thickness dependence of the charge-carrier scattering relaxation time τ assuming equal roughness (equal $U^2\rho_s$) of all slab thicknesses d. In case of diffuse elastic scattering, τ is independent of the subband index n and electron momentum $\boldsymbol{k}$. Experimental points are given by equation (5) where the experimental conductivities $\sigma_0^{\exp}$ are from reference [18]. Dashed line is a linear fit to the experimental points.

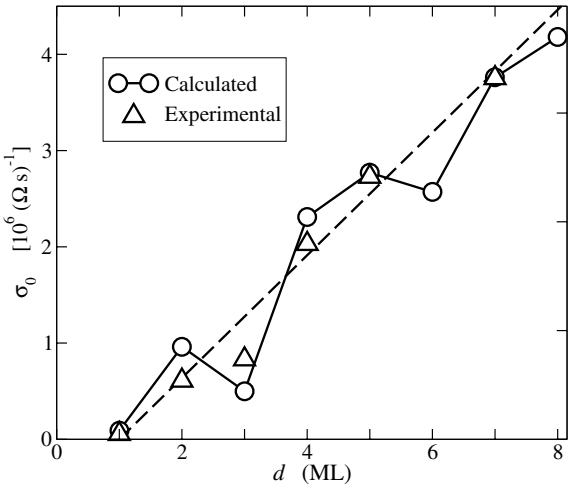

Fig. 7. Thickness dependence of the calculated (Eq. (1)) and low-temperature experimental [18] conductivity σ_0. Notice the remarkable similarity between σ_0 and τ which is the consequence of linear thickness dependence of L, Figure 6. Dashed line is a linear fit through the experimental points. (In Fig. 2 of Ref. [18] σ_0 must be multiplied by a factor 100.)

There have been several attempts to relate the Hall coefficient to the electron density of states, in particular for disordered metals [25]. Therefore we decided to test the above relations. In Figure 9 we show the dependence of calculated σ_0/τ and σ_H/τ^2 on the position of the Fermi level for a $d = 4$ ML slab. We artificially shift the Fermi energy and calculate the corresponding $\sigma_0/\tau(\epsilon_F)$ and $\sigma_H/\tau^2(\epsilon_F)$. As is seen from this figure, σ_0/τ is a relatively smooth function of ϵ_F whereas σ_H/τ^2 oscillates strongly with ϵ_F and changes sign: it is negative at the bottom of each subband, when the charge carriers are

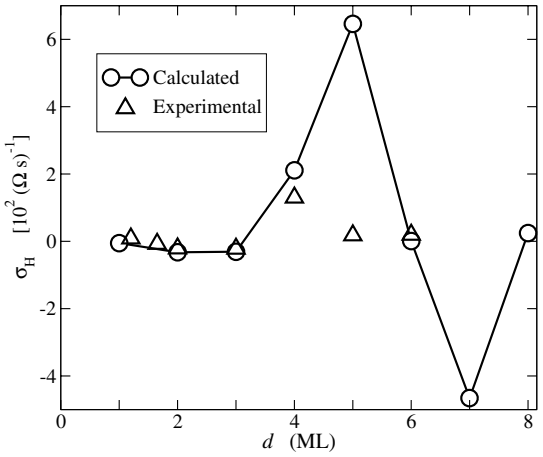

Fig. 8. The calculated Hall conductivity σ_H, equation (2), is compared to the experimental Hall conductivity, $\sigma_H^{\exp} = R_H(\sigma_0^{\exp})^2$. Huge oscillations are the effect of cancellations between electron and hole contributions.

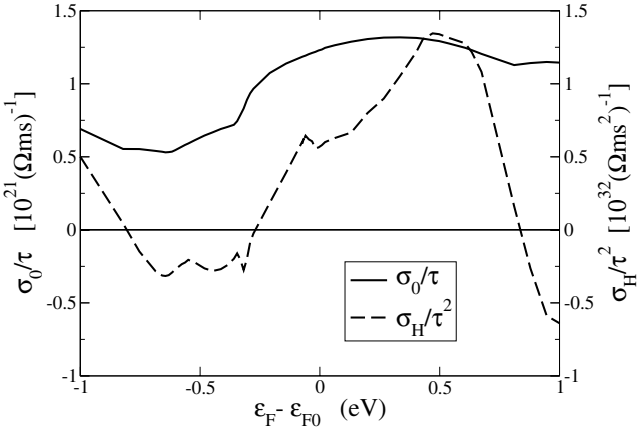

Fig. 9. Energy dependence of the calculated electrical conductivity σ_0/τ and Hall conductivity σ_H/τ^2 for a 4 ML thick slab.

electron-like, and positive at the top of the subbands when the carriers are hole-like. In between, they are complicated functions of the Fermi energy and reflect different singularities in the bandstructure. As a consequence, the dependence of R_H on ϵ_F is given predominantly by σ_H/τ^2. Comparison of $\sigma_H/\tau^2(\epsilon_F)$, Figure 9, and of the density of states, Figure 4b, shows that for $d = 4$ ML, there is no evident relation between R_H and the density of states. Such a relation would be valid only if we had a single three-dimensional band, i.e. when the charge carriers at the bottom (top) of the band are electrons with $R_H < 0$ (holes with $R_H > 0$) and at the same time the density of states is a rising (falling) function of the energy. In case of several inter-penetrating bands, as is the case of thin films, such a simple picture breaks down [26–28], as is also obvious from our results. We also find no obvious relation between σ_0 and the density of states.

4 Comparison with the experiments

In Figures 6 and 7 we compare calculated τ and σ_0 with the experiments. It has been observed experimentally that

the transport properties of Pb films are almost independent of the substrate reconstruction [18]. Therefore, metals on Si can be considered to a reasonable first approximation as free-standing metal films. This is not true for the first Pb layer, which will be discussed separately below.

Clearly seen in theory and experiments is an approximately linear thickness dependence of σ_0 which corroborates the picture that the scattering is dominated by surface roughness and that the roughness does not change with film thickness.

We identify several conductivity regions. Below the percolation threshold at $d \sim 0.8$ ML the charge carriers are localised, the transport is strongly temperature activated and σ_0 is so small that it is of no relevance for our considerations.

Between the percolation threshold and 1 ML the Pb films are pseudomorphous, i.e. the lattice constant is ∼10% larger than the corresponding bulk Pb value. We performed also DFT and conductivity calculations for a $d = 1$ ML thick Pb slab with the lateral lattice constant of a Si(111) substrate and we find that the electrical properties of a 1 ML film are extremely sensitive to the lateral lattice constant a. A 10% increase in the lattice constant changes the metal to an indirect bandgap semiconductor. The experimental conductivity of a 1 ML film is very small and has an approximately linear temperature dependence [18], supporting the theoretical conjecture that the 1 ML Pb(111) films are semiconducting.

Between ∼1 ML and ∼3.5 ML, the annealed films are amorphous and $\sigma_0^{\rm exp}$ exhibits a small, almost linear increase with temperature up to ∼100 K, indicating a small activated contribution. Films with $d \gtrsim 4$ ML are crystalline and $\sigma_0^{\rm exp}$ decreases with increasing temperature (phonons). We could not observe any influence of disorder on the conductivity of ultrathin films. The experimentally observed dip in σ_0 at 3 ML (see Fig. 7) is fully reproduced in our calculation with ideally ordered slabs. It is related to the electronic bandstructure, but has nothing to do with disorder in the film. Therefore, it is a pure quantum-size effect.

The thickness dependence of σ_0 is, like τ, $\propto d-1$. It is governed by scattering on the surface or interface roughness – bulk disorder would give a thickness-independent σ_0. The main source of the oscillations of σ_0 with d is the quantisation of the Pb band structure in the direction normal to the film together with the strong spin-orbit interaction.

Our results for σ_0 are consistent with the picture that the electrons are subject to diffuse elastic scattering at the surfaces of the films [1,2,4], in agreement with the original Fuchs-Sondheimer model, but they are at variance with the model of scattering at surfaces with uncorrelated roughness, where $\sigma \propto d^2$ was predicted [10].

The calculated Hall conductivity is compared to $\sigma_H^{\rm exp}$ in Figure 8. The agreement is good except for $d = 5$ ML where the discrepancy most probably lies in the lifetime broadening of the electron states [18] which is neglected in the present analysis.

5 Discussion

Our calculation used for the interpretation of the experimental data is based on a DFT band structure calculation combined with the Boltzmann transport equation. The only adjustable parameter, used in the calculation, is the scattering strength $U^2\rho_s$. The physical scenario is described by electronic states in ultrathin films that are localised in the direction normal to the surface and are scattered by surface roughness. The electron states form discrete subbands since the electron coherence length, limited by scattering in the film bulk, exceeds the film thickness.

The results of the calculation are consistent with the picture that the electrons are subject to diffuse elastic scattering on film surfaces [1,2,4] for which σ_0 and τ are proportional to the number of conducting metallic layers, in our case $(d-1)$, in agreement with the original Fuchs-Sondheimer model and with the experiments [18]. The (lateral) mean free path of electrons in Pb ultrathin films on Si(111) exceeds the Pb bulk lattice constant when $d > 1$ ML. According to the Ioffe-Regel criterion [29], $l \sim 1/k_F \sim a_b$ (a_b is the bulk lattice constant), the electrons in $d > 1$ ML thick films are not localised, and the use of the Boltzmann transport equation is justified.

The essential difference between the Fuchs-Sondheimer and the present model is that in the former the electrons are described by three-dimensional Bloch states whereas in our approach the electron states are described by two-dimensional momenta $k_\parallel$ and discrete subbands. The former approach is adequate for thick slabs, whereas our approach is valid for ultrathin slabs when the electron coherence length exceeds the slab thickness d.

In experiment, no free-standing films can be investigated, i.e. an insulating substrate is always required that tries to impose its own periodicity on the adsorbed film, depending on the interface energies, and on lattice mismatch. For a perfect film, an atomically sharp interface and a well defined periodicity at the interface are required (e.g., in form of a superstructure). In the Pb/Si(111) case, where the lattice mismatch is approximately 10%, no lattice match, apart from the first monolayer, can be expected. This is the reason for the formation of the amorphous films up to 4 monolayers, whose many degrees of freedom are obviously needed to allow for the growth of a Pb film with its own lattice constant for thicker layers. Nevertheless, it seems that the short range order in these amorphous films is still sufficiently good to allow a comparison of conductivity and Hall conductivity calculated for perfect crystalline order with experimental data obtained in amorphous films. The calculations with perfectly ordered films even reproduce details of the conductivity as a function of layer thickness.

As seen from our analysis, the diffuse interface scattering mechanism still limits the conductivity, even for the crystalline films at larger d. For crystalline layers the interface to the vacuum is atomically smooth for complete layers, but can be roughened by adsorption of incomplete layers, as seen by a reduction in conductivity [24]. These roughness-induced changes of conductivity, however, are

small. Therefore, the Pb-vacuum interface does not seem to provide the main contribution to diffuse scattering for the crystalline Pb films (the terraces are too large and their density too small). An electronically still very rough interface, on the other hand, may exist between the crystalline and the amorphous layers. Because of the lack of order in the amorphous state, this interface scatters at random in all directions, i.e. it still acts as diffusely scattering interface. Additional contributions to electron scattering from the Si-Pb interface are conceivable.

The single pseudomorphous monolayer of Pb on Si(111) has a narrow indirect band gap and is thus semiconducting, according to the DFT calculations, in agreement with the experiments, where the conductivity has an approximately linear temperature dependence [18]. This is not the case for free-standing Pb monolayers, which correspond to Pb deposited on semiconducting 1 ML Ag-covered Si(111)($\sqrt{3}\times\sqrt{3}$) [17], where Pb still has a Fermi line and is thus, strictly speaking, a metal, but with a very small conductivity.

6 Conclusions

Our analysis of the charge-carrier scattering and transport in ultrathin metallic Pb films has shown that they are very sensitive to the reduced dimensionality of ultrathin layers resulting in classical and quantum size effects. The relaxation time τ and the conductivity σ_0 are limited by the scattering on rough surfaces and are approximately linear functions of d (classical size effect) with quantum-size induced deviations from linearity at $d = 3$, 6 and 8 ML. The proportionality constant in $\sigma_0 \propto (d-1)$ depends on roughness of the interface to the substrate. The deviations for $d = 3, 6$ and 8 ML appear when the Fermi energy coincides with a local maximum in the electron density of states and causes a drop in τ. These deviations are the analogue of the condition $id \approx j\lambda_F/2$ (where i and j are integers and λ_F the Fermi wave length) in the free electron model [5,6]. R_H is very sensitive to details of the bandstructure and to a large extent insensitive to disorder in the film and to surface roughness.

As demonstrated in this paper, the charge-carrier transport is very suitable for investigating the QSE, since it is to a large extent insensitive to disorder in the film and is limited by the interface roughness.

The quantum-size-induced oscillations of σ_H and R_H are strong and originate from partially compensating contributions to the Hall conductivity that emerge from different subbands crossing the Fermi energy. The advantage of R_H over σ_H is that R_H is almost insensitive to the charge-carrier lifetime and consequently to ordering in the film.

Whereas one ML of free-standing Pb slab is metallic, a single monolayer of Pb, pseudomorphous with Si(111), is semiconducting. In both cases, however, the conductivity and the mean free path are small. The band gap in the pseudomorphous case is caused by spin-orbit splitting.

The method applied here can be used for other ultrathin metallic films, provided the electron coherence length (or mean free path) is larger than the film thickness. We have shown that the quantum-size effects depend on the details of the electronic bandstructure and cannot be treated quantitatively with the free electron models, in particular in case of heavier metals when the spin-orbit interaction is strong. This applies also to σ_H which is very sensitive to details of the bandstructure.

This work was supported by grants from the Deutsche Forschungsgemeinschaft, from the Deutsche Akademische Austauschdienst and from the Slovenian MSZS.

References

1. K. Fuchs, Proc. Cambridge Philos. Soc. **34**, 100 (1938)
2. E.H. Sondheimer, Adv. Phys. **1**, 1 (1952)
3. J.R. Sambles, Thin Solid Fims **106**, 321 (1983)
4. H.E. Camblong, P.M. Levy, Phys. Rev. B **60**, 15782 (1999)
5. V.B. Sandomirskii, Zh. Eksp. Teor. Fiz. **52**, 158 (1967); [Sov. Phys. JETP **25**, 101 (1967)]
6. N. Trivedi, N.W. Ashcroft, Phys. Rev. B **38**, 12298 (1988)
7. G. Govindaraj, V. Devanathan, Phys. Rev. B **34**, 5904 (1986)
8. Z. Tešanović, M.V. Jarić, S. Maekawa, Phys. Rev. Lett. **57**, 2760 (1986)
9. G. Fishman, D. Calecki, Phys. Rev. Lett. **62**, 1302 (1989)
10. D. Calecki, Phys. Rev. B **42**, 6906 (1990)
11. A.E. Meyerovich, A. Stepaniants, J. Phys.: Condens. Matter. **12**, 5575 (2000)
12. P. Joyez, D. Esteve, Phys. Rev. B **64**, 155402 (2001)
13. G. Palasantzas, J.Th.M. De Hosson, Phys. Rev. B **63**, 125404 (2001)
14. P. Saalfrank, Surf. Sci. **274**, 449 (1992)
15. G. Materzanini, P. Saalfrank, P.J.D. Lindan, Phys. Rev. B **63**, 235405 (2001)
16. M. Jałochowski, E. Bauer, Phys. Rev. B **37**, 8622 (1988); M. Jałochowski, E. Bauer, Phys. Rev. B **38**, 5272 (1988); M. Jałochowski, E. Bauer, H. Knoppe, G. Lilienkamp, Phys. Rev. B **45**, 13607 (1992)
17. M. Jałochowski, M. Hoffmann, E. Bauer, Phys. Rev. Lett. **76**, 4227 (1996)
18. I. Vilfan, M. Henzler, O. Pfennigstorf, H. Pfnür, Phys. Rev. B **66**, 241306 (2002)
19. J.P. Perdew, Y. Wang, Phys. Rev. B **45**, 13244 (1992)
20. P. Blaha, K. Schwarz, G.K.H. Madsen, D. Kvasnicka, J. Luitz, WIEN2k, a full potential LAPW package (K. Schwarz, TU Vienna, 2001)
21. E. Sjöstedt, L. Nordström, D.J. Singh, Solid State Comm. **114**, 15 (2000)
22. D.J. Singh, *Plane waves, pseudopotentials, and the LAPW method* (Kluwer Academic, Boston, MA, 1994)
23. W.W. Schulz, P.B. Allen, N. Trivedi, Phys. Rev. B **45**, 10886 (1992)
24. O. Pfennigstorf , A. Petkova, H.L. Günter, M. Henzler, Phys. Rev. B **65**, 45412 (2002)
25. A. Houari, M. Mebrouki, A.F.R. Dib, F. Ould-Kaddour, Physica B **291**, 387 (2000)
26. G. Busch, J.J. Guntherrodt, Solid State Phys. **29**, 335 (1974)
27. B. Movaghar, in *Physics of Disordered Materials*, edited by D. Adler et al. (Plenum, New York, 1985)
28. D. Nguyen-Manh, D. Mayou, G.J. Morgan, A. Pasturel, J. Phys. F: Met. Phys. **17**, 999 (1987)
29. A.F. Ioffe, A.R. Regel, Prog. Semicond. **4**, 237 (1960)